RSC Advances

This is an *Accepted Manuscript*, which has been through the Royal Society of Chemistry peer review process and has been accepted for publication.

Accepted Manuscripts are published online shortly after acceptance, before technical editing, formatting and proof reading. Using this free service, authors can make their results available to the community, in citable form, before we publish the edited article. This *Accepted Manuscript* will be replaced by the edited, formatted and paginated article as soon as this is available.

You can find more information about *Accepted Manuscripts* in the Information for Authors.

Please note that technical editing may introduce minor changes to the text and/or graphics, which may alter content. The journal's standard Terms & Conditions and the Ethical guidelines still apply. In no event shall the Royal Society of Chemistry be held responsible for any errors or omissions in this *Accepted Manuscript* or any consequences arising from the use of any information it contains.

ROYAL SOCIETY OF CHEMISTRY

www.rsc.org/advances

Encrustation of cobalt doped copper ferrite nanoparticles on solid scaffold CNTs and their comparison with corresponding ferrite nanoparticles: A study of structural, optical, magnetic and photo catalytic properties

Charanjit Singh[a], S. Bansal[b], Vinod Kumar[c], K. B. Tikoo[c], Sonal Singhal[a,*]

[a]Department of Chemistry, Panjab University, Chandigarh, India-160014

[b]Department of Science and Technology, New Delhi

[c]ICON Analytical Equipment (P) Ltd., Mumbai - 400018, India

[*]sonal1174@gmail.com

Abstract

Cobalt doped copper ferrite nanoparticles and their nanocomposites with carbon nanotubes (CNTs) were synthesized by microemulsion method where sodiumdodecylsulphate was used as soft templating agent to control the particle size and shape. Powder X-ray diffraction technique confirmed the formation of cobalt doped copper ferrite nanoparticles and their corresponding nanocomposites. A significant decrease in the lattice parameter was observed using Le-bail refinement method which confirmed the doping of cobalt ion in to the copper ferrite lattice. Appearance of peak at around 25.9° indicated that CNTs remain unaffected during synthesis procedure. High Resolution Transmission Electron Microscopy (HR-TEM) was used to estimate the particle size, shape and uniformity of all the synthesized samples. Particle size was observed to be around 4-5 nm. A fine layer of ferrite nanoparticles on the surface of CNTs was also confirmed. Optical studies of the entire samples showed wide coverage of visible light spectrum from 675-1050 nm. Magnetic studies of the all samples were carried out using Vibrating Sample Magnetometer and a significant increase in the saturation magnetization and coercivity values

RSC Advances Accepted Manuscript

with cobalt ion doping was observed. This increase could be attributed to the higher magnetic moment of Co^{2+} ions (3 μB) as compared to Cu^{2+} ion (1 μB) at B-sub lattice. Comparative photocatalytic activity was also elevated and it was found that ferrite-CNTs nanocomposites show higher catalytic activities for the degradation of Rhodamine B dye in comparison with the ferrite nanoparticles.

Key word: Composite materials, Electron microscopy, Magnetic properties, Optical spectroscopy

1. Introduction

Research groups have explored the vital use of these nano ferrites in numerous advanced techniques due to their unique physical and chemical properties[1-3]. Nano dimension of iron oxide materials completely change their domain of operation and working in the field of magnetism, optics, catalysis and wave absorbers[4-6]. Particles of ferrite in nano range show an extraordinary behavior in comparison to their bulk counterparts. However, strong urge of ferrite nanoparticles to agglomerate has been considered as a major problem which deprives their application in the field of nanofluids, drug delivery and heterogeneous catalysts.[7, 8]

Particle aggregation, nano-range stability with defined shape and size uniformity has been vitally reliant on synthetic strategy. Reverse micelle synthesis has an asset over other synthetic protocols in aspects of narrow size distribution, stability, confined particle dimensions and controlled shape of ferrite nanoparticles. Further, nanoferrite have been encrusted over the various solid scaffold matrices such as silica, carbon nanotubes, zeolites and polymer materials so as to improve their applicability and enhance their nano range stability.[9-12]

RSC Advances Accepted Manuscript

So, substitution of suitable transition metal ion into the lattice of spinel ferrite, its synthesis methodology and attachment with apposite solid scaffold matrix brings revolutionary change in the properties of heterojunction composites.

It is interesting to study the substitution of cobalt ion at the octahedral site of the copper ferrite spinel structure through micro-emulsion synthesis. Further, cobalt doped copper ferrite nanoparticles[13-15] can be ensheathed on the reflective curved surface of CNTs which give rise to synergistic effect. Thus, so produced synergistic effect, amazingly change their behavior in the desired direction providing complete stabilization to nanoparticles on solid support medium[16, 17]. Such heterojunction nanocomposites behave as a single entity which retains the properties of both adjoining materials. Also, the issue of stability of tiny nano magnets of metal doped ferrites has been resolved by providing a suitable platform for growth.

Various research groups have encrusted the ferrite nanoparticles on the surface of CNTs and graphene. Zhou et al.[18] attached the cobalt ferrite nanoparticles of around 20-30 nm size on the surface of CNTs by one pot polyol method. Huge lumps of ferrite nanoparticles were grown on the surface of tubes**.** Unal et al.[19] reported the loading of super paramagnetic cobalt ferrite nanoparticles on the surface of carboxyl functionalized CNTs using co-precipitation method. The surface oxidized CNTs provided a strong adhesion between the nanotubes and the homogeneous cobalt nanoferrite. Value of saturation magnetization was 11.5 emu/g. Jiang et al.[20] decorated the cobalt ferrite nanoparticles on the surface of CNTs using polymer wrapping technique. Poly sulfostyrene with negatively charge polyelectrolyte was first grafted on the surface of carbon nanotube, which then absorbed the ferrite nanoparticles efficiently on the tube surface. Saturation

RSC Advances Accepted Manuscript

magnetization value of as obtained ferrite-CNT nanocomposite was 29.6 emu/g with negligible coercivity which pointing towards their super paramagnetic behavior.

Similar synthesis techniques were employed to axially decorate mixed spinel ferrite nanoparticles on the tubular surface of carbon. Chen et al.[21] synthesized the zinc doped cobalt ferrite-CNT nanocomposite with solvothermal method. However, aggregation of ferrite nanoparticles in the form of lumps of around 100 nm was observed from the Transmission Electron Microscope (TEM) images.

Considering the above mentioned problems of agglomeration, irregular size distribution and inadequate attachment of ferrite nanoparticles on solid matrix, this paper reports the synthesis of stoichiometric doping of cobalt ion in the surface exposed octahedral sites of copper nanoferrite sub-lattice and their encrustation on CNTs using low cost microemulsion technique. Comparative structural, optical, magnetic and photo-catalytic properties of nanoferrite and their MWCNTs (Multiwalled carbon nanotubes) nanocomposites have been scrutinized. All the samples were thoroughly investigated using Powder X-ray Diffraction, EDX (Energy Dispersive X-ray Spectroscopy), WDXRF (Wavelength Dispersive X-ray Florescence Spectroscopy). Nanoferrite tethered on reflective MWCNTs surface was analyzed using HR-TEM (High Resolution Transmission Electron Microscopy) and Raman spectroscopy. A comparative photocatalytic behavior of the pure cobalt doped copper ferrite and their nanocomposite with CNTs was evaluated for the RhB dye degradation.

2. Experimental

2.1. Materials

RSC Advances Accepted Manuscript

Cobalt chloride hexahydrate ($CoCl_2 \cdot 6H_2O$, 97%), copper chloride tetrahydrate ($CuCl_2.4H_2O$, 98%), ferric chloride ($FeCl_3$, 99.5%), sodium dodecyl sulfate (SDS, 90%), sodium hydroxide (NaOH, 98%), sulphuric acid (H_2SO_4, 98%), hydrogen peroxide (H_2O_2, 30% w/v) and Rhodamine B (99.7%) were purchased from Loba Chemicals, Chandigarh, India and were used without further purification. Absolute ethanol (C_2H_5OH, 99.9%), 1-butanol ($C_4H_{10}O$, 99.7%) and n-hexane (C_6H_{14}, 99.7%) were purchased from Fisher Scientific, Chandigarh, India. Graphite rods (5mm x 150mm) were purchased from Popular Science Apparatus Workshops Pvt. Ltd. Ambala, India. Deionized water was obtained using an ultrafiltration system (Milli-Q, Milipore) with the measured conductivity of 35 mho cm^{-1} at 25 °C.

2.2. Physical measurements

The powder X-ray Diffractometer (XRD) D8 advanced, from Bruker, of scan type locked coupled, scan angle 20 - 80° range, scan step 0:02°, scan speed 3°/min, maximum power 40kV /40mA, Cu tube, T/T horizontal was used to analyze the phase purity of the synthesized samples. The scan time for each sample was about 20 minutes and the wavelength of Cu-Kα target was 1.5406 Å. DIFFRAC-plus TOPAS, version 2.1 technical reference software was used to calculate the dimensional changes in the lattice parameter. The Fourier-Transform Infrared (FT-IR) spectra for all the samples were recorded by FT-IR instrument (PERKIN ELMER) using KBr pellets in the range 4000-400 cm^{-1}. High Resolution Transmission Electron Microscope (HR-TEM) images were recorded using FEI Technai G2 F20 operated at 200 keV with magnification of 6 x 10^6 times and resolution of 0.2 A°. Optical properties were analyzed using the UV–VIS spectrophotometer (Analytikjena SPECORD-205). The magnetic properties were measured at room temperature by a Vibrating Sample Magnetometer (VSM) (155, PAR) up to a

RSC Advances Accepted Manuscript

magnetic field of ±10kOe. Photo catalysis was performed using visible light irradiation setup. Visible light irradiation set up consisted of 160 W mercury lamp having light intensity of 96000 lux. Photo-irradiated set-up is kept in perpendicular direction having a distance of 6 inches between the light source and target surface (dye solution).

2.3. *Preparation of cobalt doped copper ferrite nanoparticles*

Cobalt doped copper ferrite nanoparticles were prepared using microemulsion technique. In this method, two micro emulsion systems were prepared using water: sodiumdodecylsulphate: hexane: 1-butanol (89.82: 3.03: 1.637: 5.568, w/w) in appropriate weight ratio[22]. These two microemulsion systems were stirred for 15 min until the solution became transparent which confirmed the formation of stable emulsion. Metals salts in stoichiometric proportion were dissolved in microemulsion system 1 and 20 ml of 5 M sodium hydroxide as a precipitating agent was dissolved in the microemulsion system 2. These two emulsions systems were then slowly mixed and kept on vigorous stirring for 1 hour with magnetic stirrer at room temperature. Brown colored precipitates were formed which indicated the formation of metal hydroxide. These precipitates were further filtered and washed using deionized water and ethanol. As obtained sample were then air dried and then kept in muffle furnace at 400 °C for 5 hours for the annealing which formed the stable ferrite nanoparticles.

2.4. *Preparation of cobalt doped copper ferrite-MWCNTs nanocomposites*

For the synthesis of cobalt doped copper ferrite-MWCNTs nanocomposites, firstly MWCNTs were prepared using arc discharge method[23] which were further washed using deionized water and ethanol and then air dried. Amorphous carbon was removed by keeping the dried sample in furnace at a temperature of 400 °C for 30 min with a ramp rate of 10 °C/min.

RSC Advances Accepted Manuscript

CNTs were further purified and functionalized by refluxing in 8M nitric acid. As obtained carbon nanotubes had negative charged carboxyl and hydroxyl functional groups on the surface. Further, 200 mg of functionalized CNTs were dispersed in the microemulsion system 1 along with the metal salt solution. 5M NaOH (40 ml) was dissolved in the microemulsion system 2. These two systems were mixed and magnetically stirred for 1 hour at room temperature. Precipitates of metal hydroxide tethered on the CNTs surface were washed with deionized water and ethanol and filtered using 0.22 micron filter membrane. Thus as obtained samples were air dried overnight and then annealed at 400° C for 5 hours. Yield of the nanocomposites so obtained is 1.25 gm[24].

2.5. Photocatalytic activity

Catalytic activities of cobalt doped copper ferrite and their corresponding nanocomposites were evaluated for the degradation of Rhodamine B (RhB) dye as standard pollutant. Firstly, 50 μM of RhB dye (100 mL) solution was prepared and the pH of this solution was adjusted to 2.5. This solution was kept in dark for 30 min so as to achieve the adsorption-desorption equilibrium. In order to generate the photo-fenton reagent, 100 μL of H_2O_2 (30% w/v) and 50 mg of the nanoferrite catalyst was added to the dye solution prior to irradiation. The solution was then kept under visible light lamp with continuous magnetic stirring. To study the time dependent degradation of dye, 2 ml of the aliquots were withdrawn from the solution at regular intervals of time. The catalyst was removed from the sample using syringe filter membrane and then UV-Visible spectra were recorded for all the aliquots to study the degradation.

3. Results and discussion

3.1. Fourier transform infra-red (FT-IR) and Raman spectroscopy

RSC Advances Accepted Manuscript

FT-IR spectroscopy confirmed the formation of M-O bond in ferrite nanoparticles. The FT-IR spectra for the entire ferrite composition are shown in fig S1 (ESI file). Appearance of sharp band at 550 cm^{-1} was due to the presence M-O bond corresponding to the metal ion present in the tetrahedral sites. The band due to the M-O bond corresponding to the metal ion present in the octahedral sites could not be observed. This could be due to the reason that sometimes the band corresponding to octahedral site stretching appear below 400 cm^{-1}. The attachment of ferrite nanoparticle with CNTs was also confirmed. Functionalization of CNTs with carboxyl group was confirmed by the appearance of band at 1745 cm^{-1} which is the characteristic peak for the carboxylic group, which appeared in the FT-IR spectra of nitric acid treated CNTs [18]. The appearance of band at same position around ~550-600 cm^{-1} was observed in the ferrite-CNTs nanocomposite heterojunction as shown in fig 2S (ESI file) which matches well with the literature reported values[25]. Raman spectra of $Cu_{0.4}Co_{0.6}Fe_2O_4$-MWCNTs nanocomposite is shown in fig 3S (ESI file). Appearance of the D-band and G-band around 1348 and 1578 cm^{-1} with an emergence of shoulder peak around 1621 cm^{-1} confirms the presence of highly pure CNTs. Presence of $Cu_{0.4}Co_{0.6}Fe_2O_4$ is confirmed from raman scattering peaks around 478, 539 and 655 cm^{-1}. High frequency peaks (650-700 cm^{-1}) corresponds to the tetrahedral mode of vibration of mixed spinel structure of ferrite whereas low frequency vibration (450-650 cm^{-1}) relates to the octahedral site of the ferrite structure.

3.2. Powder X-ray diffraction (XRD) characterization

Phase formation of cobalt doped copper ferrite nanoparticles and their nanocomposites were thoroughly investigated using Powder X-ray Diffraction technique. Fig. 1 shows the diffraction pattern of cobalt doped copper ferrite nanoparticles annealed at 400 °C.

RSC Advances Accepted Manuscript

The diffraction peaks correspond to (2 2 0), (3 1 1), (4 0 0), (4 4 0) and (5 1 1) lattice planes of cobalt doped copper ferrite which exhibited face centered cubic crystal structure[26] with Fd-3m space group and XRD results are in good agreement with JCPDS-00-001-1121. Similarly, nanocomposites of cobalt doped copper ferrite with CNTs indexed the same lattice planes as that for ferrite nanoparticles with an additional peak corresponding to (002) plane of hexagonal shape CNTs. Appearance of (002) plane in the nanocomposites clearly indicated that CNTs remain unaffected during the microemulsion treatment followed by annealing at 400 °C. A very small peak corresponding to CuO was also observed for the case of pure copper ferrite nanoparticles and CNTs nanocomposites. With the Co^{2+} ion doping into the copper ferrite, lattice peak corresponding to CuO disappeared as shown in Fig 2.

In order to calculate the crystallite size for the ferrite nanoparticles and their corresponding CNTs nanocomposites, scherrer's formula was applied[27].

$$d = K\lambda/\beta \cos\theta_B$$

where d is the average crystallite size, K is the shape factor approximated to 0.9, β is the line broadening at half the maximum intensity (at full width half of maximum intensity, FWHM), λ is the X-ray wave length. Crystallite size was calculate using the most broad and intense peak at 35.4° in both the cases. Broadness in the peak was due to smaller average crystallite size. Table 1. lists average crystallite size and the lattice parameter value for ferrite nanoparticles and their CNTs nanocomposites.

Calculation of lattice parameters for ferrite nanoparticle is an important study which significantly confirms the suitable metal ion doping in the lattice of spinel ferrite nanoparticles. Le-bail refinement method was used to calculate shifting in the lattice parameter of cobalt doped

RSC Advances Accepted Manuscript

copper ferrite nanoparticles. A small shifting in the lattice parameter for cobalt doped copper ferrite nanoparticles and their CNTs nanocomposites was observed as shown in the fig 2(a, b). Lattice parameter decrease with the cobalt ion doping in the copper ferrite nanoparticles which is due to the smaller ionic radii of the Co^{2+} ion (0.65 A°) as compared to the Cu^{2+} ion (0.73 A°).[26]

3.3. HR-TEM, EDX and WDXRF Characterization

The shape and morphology of the entire ferrite composition and CNTs encrusted with the ferrite nanoparticles were studied using HR-TEM analysis. Before analysis, synthesized MWCNTs (2 mg) were well dispersed in ethanol (20 ml) using high frequency sonication for 20 minutes. A drop of as prepared sample was put on the copper grid. Grid was allowed to air dried for 10 minutes and similarly ferrite-MWCNTs sample was agitated ultrasonically in ethanol for 20 minutes to avoid aggregation of the samples. The shape and morphology of the functionalized CNTs is shown in fig 3(a).

Large numbers of CNTs were perfectly entangled in the form of bundles along with some individual tubes. The size of these bundles was observed to be around 150 nm whereas the size of the individual nanotube was around 20 to 30 nm. Round shaped fullerene were also seen in the TEM image which was produced as a byproduct in a very trace amounts. Scattered Area Electron Diffraction (SAED) pattern of CNTs showed the (002) lattice plane which matches well with the data corresponding to the planes provided by powder XRD. Fig 3(b, c and d) shows the nanoparticles of cobalt doped copper ferrite at different resolution depicting the morphology and shape of ferrite nanoparticles. Ferrite nanoparticles were observed to be of around 4-5 nm size with a spherical shape. Fig 3(b) shows the ferrite nanoparticles at low resolution and some amount of aggregation can be seen in the image. Anyhow, when the instrument was operated at

RSC Advances Accepted Manuscript

high resolution of around 2 to 5 nm, different boundary walls of ferrite nanoparticles were clearly observed. Thus, microemulsion method plays a crucial role in the nanoparticles dispersity due to the presence of nano water pools in emulsion where the metal salts and precipitating agent reacts in the constrained boundaries[28]. The deposition of these synthesized nanoparticles on the surface of carbon scaffold matrix i.e nanotubes is shown in Fig 4.

TEM images of the ferrite-CNTs nanocomposites showed an interesting result that a fine layer of ferrite nanoparticles are completely covered the surface of CNTs. Although, some ferrite nanoparticles were not attached on the surface of tubes and can be seen on the grid as well. This could be due to smaller amount of CNTs used or strong sonication of the nanocomposite sample. Lumps of ferrite nanoparticles as reported by chen et al.[27] are not present in the nanocomposite samples as can be seen in the images which clearly indicated fine encrustation of ferrite nanoparticles on the tube surface. SAED pattern of cobalt doped copper ferrite-MWCNTs nanocomposites showed the good crystallinity with three concentric rings corresponding to the (311) and (440) plane of ferrite nanoparticles and (002) plane of the CNTs. Interlayer spacing in the ferrite nanoparticles can be calculated using the profile of frame. The distance between the two consecutive peaks represent the interlayer spacing which came out to be 0.21, 0.25 and 0.29 nm for the ferrite nanoparticles whereas for the CNTs, the values of the interlayer distance was around 0.33 nm as shown in Fig 4(e).

EDX spectrum, shown in fig 4S (ESI file), indicated that the obtained samples were composed of Cu, Co, Fe and O elements. However, a very small peak of sulfur (0.7%) appeared in ferrite-CNTs nanocomposites which could be due to the incomplete removal of surfactant. WDXRF spectrum of the $Cu_{0.4}Co_{0.6}Fe_2O_4$-MWCNTs nanocomposite is shown in fig 5. It is clear from that entire elemental composition exists in the definite stoichiometry. Iron, cobalt an copper

RSC Advances Accepted Manuscript

having higher kα1 are found in the 2: 0.6: 0.4 ratio (47.0%: 14.3%: 10.2%) in the sample. However, carbon and oxygen is not appeared in the spectra due to lower kα1 energy values which are confirmed by the raman spectroscopy and EDX analysis..

3.4. *Diffused UV-Visible Reflectance Spectra $Co_xCu_{1-x}Fe_2O_4$ nanoparticles*

Optical properties of MWCNTs, cobalt doped copper ferrite nanoparticles and their corresponding CNTs nanocomposites were analyzed by diffused UV-Visible reflectance spectroscopy. Band edge absorption for all the samples was calculated using this technique which assigns a range for absorption of suitable wavelength from the solar spectrum. Diffused UV-Visible spectra of MWCNTs depicted in fig 5S (ESI file) and it is clear that CNTs have negligible absorption in the visible region. Fig. 6(a) shows the band edge absorption spectra of cobalt doped copper ferrite nanoparticles for different values of Co^{2+} ions as a dopant. The absorbance results demonstrated that Cu-Co ferrite nanoparticles had significant absorbance in 825-1050 nm wavelength range of the visible region which was important for photo catalytic reaction. Band edge absorption onset for copper ferrite was at 825 nm and with the Co^{2+} ion doping the edge absorption value sequentially increased. Absorption edge values found for $Co_xCu_{1-x}Fe_2O_4$ nanoparticles were 856, 902, 960 and 1050 nm for x = 0.2, 0.6, 0.8 and 1.0 respectively. Deposition of cobalt doped copper ferrite nanoparticles on the CNTs surface exhibited the solar spectrum absorption in the range of 680-995 nm as shown in Fig 6 (b). This was due to synergistic effect of CNTs with the ferrite nanoparticles which decrease their band edge absorption.

3.5. Band gap of $Co_xCu_{1-x}Fe_2O_4$ nanoparticles

The band gap energy values were estimated by a plot of $(\alpha h\nu)^2$ vs photon energy ($h\nu$). The optical absorption coefficient near the band edge follows the equation[29]:

RSC Advances Accepted Manuscript

$$\alpha h\nu = A(h\nu - E_g)^{1/2}$$

where α, h, ν, E_g, and A are the absorption coefficient, Plank's constant, light frequency, band gap, and proportionality constant, respectively. The calculation of the band gap energy involves the extrapolation of the linear part of the curve obtained by plotting $(\alpha h\nu)^2$ vs (hν) to cut the energy axis. The estimated band gap values for $Co_xCu_{1-x}Fe_2O_4$ nanoparticles were found to be 1.4, 1.44, 1.37, 1.29 and 1.2 eV for x = 0.0, 0.2, 0.6, 0.8 and 1.0 respectively. A significant change in the band gap values indicated the large range for the visible region absorption. Similarly, nanocomposites of CNTs with $Co_xCu_{1-x}Fe_2O_4$ nanoparticles had band gap value of around 1.82 eV for the copper ferrite-CNTs nanocomposite and this value decreased with increase in the cobalt ion doping in the material. Values of the band gap for cobalt doped copper ferrite-CNTs with x = 0.2, 0.6, 0.8 and 1.0 were estimated to be around 1.76, 1.70, 1.42 and 1.25 eV respectively. Increase in the band gap value of nanocomposites as compared to nanoparticles indicated the formation of energy levels or interface defects due to synergistic effect of ferrite with carbon tubes which decreased the electron hole recombination and values of band gap significantly increased[30].

3.6. A comparative Magnetic properties of $Co_xCu_{1-x}Fe_2O_4$nanoparticles and $Co_xCu_{1-x}Fe_2O_4$-MWCNTs nanocomposites

Hysteresis loops for all the samples were recorded at 298 K using VSM by applying the external magnetic field between ± 10 kOe and are shown in Fig 7.

It was observed that the saturation magnetization increased with increase in Co^{2+} ion concentration (Table 2). This behavior of saturation magnetization can easily be explained on the basis of Neel's two sub-lattice model. According to this model, the magnetic moment per formula unit in Bohr magneton $n_B^N(\chi)$ is expressed[31]:

RSC Advances Accepted Manuscript

$$n_B^N(\chi) = M_B(\chi) - M_A(\chi)$$

where M_B and M_A are magnetization of B and A sub-lattices, respectively.

The increase in the saturation magnetization was attributed to the higher magnetic moment of Co^{2+} ion (3 μB) as compared to its substituted counterpart Cu^{2+} ion (1 μB). Hence, magnetic moment at B-sub lattice sequentially increased with increase in the cobalt doping which lead to the overall increase in the magnetic moment of the sample with Co^{2+} ion doping.[26] The values of saturation magnetization, coercivity and remanance are given in Table 2.

With increase in cobalt ion doping in the copper ferrite, values of coercivity also increased monotonically. Value of coercivity was found to be 8 Oe for copper ferrite and with the cobalt ion doping, coercivity value increased significantly and reached around 510 Oe for pure cobalt ferrite. Similar trends in the saturation magnetization values were observed for the CNTs ferrite nanocomposites as shown in Fig 7 (b). However, saturation magnetization values for the nanocomposites were found to be smaller as compared to their corresponding nanoparticle counterpart. This decrease in the values of saturation magnetization could be due to the non-magnetic CNTs present in the nanocomposite sample.

3.7. Photo catalytic activity

The photo-catalytic activity of copper ferrite and the influence of stoichiometric doping of cobalt ion and introduction of solid scaffold CNTs matrix in $Co_xCu_{1-x}Fe_2O_4$ nano-particles were evaluated for the degradation of Rhodamine B (RhB) solution. The photo-irradiated setup for the photocatalysis of RhB solution is shown in fig 6S (ESI file). The UV-visible spectra of RhB solution showed characteristic peaks at a wavelength of 556 nm. It was found that copper ferrite completely degraded the RhB dye in 120 min. On addition of cobalt ion to copper ferrite lattice, the degradation rate slowly increased from x = 0.0 to 0.8 and on complete substitution of

RSC Advances Accepted Manuscript

cobalt ion into the copper ferrite lattice, sharp decrease in the initial reaction rate was observed. However, the rate of reaction for the cobalt ferrite increases sharply after 40 minutes. $Co_{0.8}Cu_{0.2}Fe_2O_4$ sample was found to have the highest rate of reaction and degrade the dye in 100 minutes. The percentage photocatalytic degradation was calculated by applying following equation[32]

$$\%\ degradation = \left(\frac{A_0 - A_t}{A_0}\right) \times 100$$

where A_o is the initial RhB concentration and A_t is the concentration of RhB at time t. Fig. 8 (a) shows the percentage degradation of the dye with time for the nano-ferrites.

Degradation rate for the nanocomposites were also studied which show significant increase in the rate of reaction. $Co_{0.8}Cu_{0.2}Fe_2O_4$-MWCNTs completely degrade the RhB dye in 60 min. An energy level diagram is depicted in the fig 9 which elaborates the effectiveness of cobalt doped copper ferrite-MWCNTs nanocomposites. Effect of CNTs for the photocatalytic activity was observed in all the nanocomposite samples. However, it was distinctively seen for cobalt ferrite. A significant change in the rate of the reaction was observed when cobalt ferrite nanoparticles were encrusted on the CNTs surface. Form the obtained results, it can be concluded that presence of CNTs significantly enhances the catalytic properties. This could be due to synergistic effect of CNTs with ferrite nanoparticles[33] which can be explained from fig 9. It is clear from energy level diagram that irradiation of CNTs yield photo-generated electrons which transferred to the copper ferrite nanoparticles. $CuFe_2O_4$ nanoparticles having band gap of 1.4 eV and electrons from the valence band of the copper ferrite excited to conduction band. After doping with the cobalt ion in the copper ferrite spinel lattice, band gap of the cobalt doped copper ferrite nanocomposite reduced (1.2 eV) and this facilitates the easy transportation of electron form higher conduction band of copper ferrite to the lower conduction band of cobalt

RSC Advances Accepted Manuscript

doped copper ferrite. So, this process restricts the electron hole recombination rate and subsequently facilitates the decomposition of H_2O_2 which produce the hydroxyl radical and decolorize the dye molecule[34].

3.8. Recyclability

Recyclability of the $Co_{0.8}Cu_{0.2}Fe_2O_4$-MWCNTs nanocomposite sample is important due to its future applicability in the degradation of organic pollutant present in various water sources. Such nanocomposites are easily separable from reaction mixture using an external magnet due to their excellent magnetic properties. So, on the completion of reaction process, an external magnet is used to drive the magnetic nanocomposite form the reaction beaker. So obtained nanocomposite sample is washed 3 times with distilled water and kept in oven at 100 °C for 5 hours. Recovered catalyst is again dispersed in RhB solution. Fig 7S (ESI file) showing no significant loss in the activity of nanocomposite sample even after five consecutive cycles.

4. Conclusion

Cobalt doped copper ferrite nanoparticles were successfully synthesized by microemulsion method and their deposition on the surface of carbon nanotubes was also accomplished and thoroughly studied using HR-TEM technique. Formation and doping of cobalt ion into the copper ferrite lattice and their corresponding nanocomposites was confirmed by Powder XRD. Optical studies of the entire samples revealed that ferrite nanoparticles absorbed the visible light in the range of 825 - 1050 nm. However, Ferrite-CNTs nanocomposites absorb the visible light in the region of 680-995 nm. Magnetic studies revealed that with cobalt ion doping, value of saturation magnetization and coercivity increased and reached a maximum value of 33.5 emu/g whereas the values for ferrite-CNTs nanocomposite were smaller. Photocatalytic properties of all

RSC Advances Accepted Manuscript

the samples were also studied and $Co_{0.8}Cu_{0.2}Fe_2O_4$-MWCNTs nanocomposite sample was found to be the most catalytically active amongst all the samples.

Acknowledgements

The authors are grateful to Department of Science and Technology (DST) and Council of Scientific and Industrial Research (CSIR) for providing the necessary financial support.

References

1. A. H. Lu, E. L. Salabas, F Schuth, Angew. Chem. Int. Ed. 2007, **46**, 1222-1244.
2. S. Shylesh, V. Schunemann, W. R. Thiel, Angew. Chem. Int. Ed. 2010, **49**, 3428-3459.
3. M. Zhu and G. Diao, Nanoscale, 2011, **3**, 2748.
4. P. Xiong, Y. Fu, L. Wang, X. Wang, Chem Engg J, 2012, **195-196**, 149-157.
5. C. A. Demarchi, A. Debrassi, F. C. Buzzi, R. Correa, V. C. Filho, C. A. Rodrigues, N. Nedelko, P. Demchenko, A. S. Waniewsk, P. Duzewski and J. M. Grenechec, Soft Matter 2014, **10**, 3441-3450.
6. A. M. Gama, M. C. Rezende, C. C. Dantas, J Magn Magn Mater, 2011, **323**, 2782-2785.
7. T. T. Baby, S. Ramaprabhu, J. Mater. Chem. 2011, **21**, 9702.
8. R. K. Singh, K. D. Patel, J. J. Kim, T. H. Kim, J. H. Kim, U. S. Shin, E. J. Lee, J. C. Knowles, H. W. Kim, 2014, **6**, 2201.
9. K. Nadeema, F. Zeb, M. Azeem Abid, M. Mumta, M. Anis ur Rehman, J. Non-Cryst. Solids. 2014, **400**, 45.

RSC Advances Accepted Manuscript

10. L. Khanna, N. K. Verma, Biocompatibility and superparamagnetism in novel silica/$CaFe_2O_4$ nanocomposite, Materials Letters 2014, **128**, 376.

11. D. Y. Park, S. T. Myung, ACS Appl. Mater. Interfaces 2014, **6**, 11749.

12. Z. Li, Y. Shen, Y. Guan, Y. Hu, Y. Lin, C. W. Nan, J. Mater. Chem. A, 2014, **2**, 1967.

13. D. Carta, M. F. Casula, A. Falqui, D. Loche, G. Mountjoy, C. Sangregorio, A. Corrias, J. Phys. Chem. C 2009, **113**, 8606.

14. C. Pereira, A. Pereira, C. Fernandes, M. Rocha, R. Mendes, M. P. Fernandez-Garcia, A. Guedes, P. B. Tavares, J. M. Greneche, J. P. Araujo, C. Freire, Chem. Mater. 2012, **24**, 1496.

15. S. Briceno, H. D. Castillo, V. Sagredo, W. B. Escamillaa, P. Silvaa, Appl. Surf. Sci. 2012, **263**, 100.

16. P. Xiong, Y. Fu, L. Wang, X. Wang, Chem. Engg. J. 2012, **195-196**, 149.

17. Y. Fua, H. Chen, X. Sun, X. Wang, Appl. Catal., B 2012, **111-112**, 280.

18. L. Zhou, L. Jia, P. C. Ma, Y. Shao, H. Zhang, W. Gao, Y. Li, J. Hazard. Mater. 2014, **265**, 104.

19. B. Unal, M. Senel, A. Baykal, H. Sozeri, Curr. Appl. Phy. 2013, **13**, 1404.

20. W. Jiang, Y. Liu, F. Li, J. Chu, K. Chen, Mater. Sci. Engg. B 2010, **166**, 132.

21. Y. Chen, X. Wang, Q. Zhang, Y. Li, H. Wang, J. Alloys Compds. 2011, **509**, 4053.

22. S. T. Hussain, S. R. Gilani, S. D. Ali, H. S. Bhatti, J. Alloys Compds. 2012, **544**, 99.

23. S. Singhal, C. Singh, P. Singla, K. Dharamvir, Solid State Phenomenon. 2013, **201**, 197.

24. C. Singh, S. Bansal, S. Singhal, Physica B 2014, **444**, 70.

25. R. Sharma, S. Singhal, Physica B 2013, **414**, 83.

26. A. Azam, J. Alloys Compds. 2012, **540**, 145.

27. A. Goyal, S. Bansal, S. Singhal, Inter. J. Hydrogen. Energ. 2014, **39**, 4895.

RSC Advances Accepted Manuscript

28. S. Kumar, V. Singh, S. Aggarwal, U. K. Mandal, Mater. Sci. Engg., B 2010, **166**, 76.

29. S. M. Chavan, M. K. Babrekar, S. S. More and K. M. Jadhav, J. Alloys Compds. 2010, **507**, 21.

30. X. Li, Y. Hou, Q. Zhao, L. Wang, J Colloid. Interf. Sci. 2011, **358**, 102.

31. S. Bhukal, T. Namgyal, S. Mor, S. Bansal, S. Singhal, J. Mol. Struct. 2012, **1012**, 162.

32. M. M. Rashad, R. M. Mohamed, M. A. Ibrahim, L. F. M. Ismail, E. A. Abdel-Aal, Adv. Powder Technol. 2012, **23**, 315.

33. C. H. Chen, Y. H. Liang, W. D. Zhang, J. Alloys Compds. 2010, **501**, 168.

34. E. Casbeer, V. K. Sharma, X. Z. Li, Sep. Purifi. Techno. 2012, **87**, 1.

RSC Advances Accepted Manuscript

Table 1. Crystallite size of $Co_xCu_{1-x}Fe_2O_4$ with different concentration of Co^{2+} ions

Nanoferrite samples	Lattice Parameter a(A°)	Average crystallite size (nm)
$CuFe_2O_4$	8.397	11.3
$Co_{0.2}$ $Cu_{0.8}Fe_2O_4$	8.393	8.1
$Co_{0.6}$ $Cu_{0.4}Fe_2O_4$	8.385	9.6
$Co_{0.8}$ $Cu_{0.2}Fe_2O_4$	8.383	6.1
$CoFe_2O_4$	8.382	5.4
$CuFe_2O_4$-MWCNTs	8.395	9.1
$Co_{0.2}$ $Cu_{0.8}Fe_2O_4$-MWCNTs	8.391	7.8
$Co_{0.6}$ $Cu_{0.4}Fe_2O_4$-MWCNTs	8.387	6.7
$Co_{0.8}$ $Cu_{0.2}Fe_2O_4$-MWCNTs	8.379	7.1
$CoFe_2O_4$-MWCNTs	8.38	5.9

RSC Advances Accepted Manuscript

Table 2. Saturation magnetization, Coercivity and remanance of $Co_xCu_{1-x}Fe_2O_4$ nanoparticles and $Co_xCu_{1-x}Fe_2O_4$/MWCNTs nanocomposites

Nanoferrite samples	Saturation magnetization M_s (emu/g)	Corecivity H_c (Oe)	Remanance M_r (emu/g)
$CuFe_2O_4$	17.3	9	0.2
$CuFe_2O_4$-MWCNTs	12.9	40	0.7
$Co_{0.2}$ $Cu_{0.8}Fe_2O_4$	19.2	160	1.5
$Co_{0.2}$ $Cu_{0.8}Fe_2O_4$-MWCNTs	15.4	120	0.8
$Co_{0.6}$ $Cu_{0.4}Fe_2O_4$	24.5	100	0.9
$Co_{0.6}$ $Cu_{0.4}Fe_2O_4$-MWCNTs	16.5	75	0.6
$Co_{0.8}$ $Cu_{0.2}Fe_2O_4$	26.2	375	4.9
$Co_{0.8}$ $Cu_{0.2}Fe_2O_4$-MWCNTs	20.6	300	8.7
$CoFe_2O_4$	33.9	500	9.7
$CoFe_2O_4$-MWCNTs	29.2	525	12.5

RSC Advances Accepted Manuscript

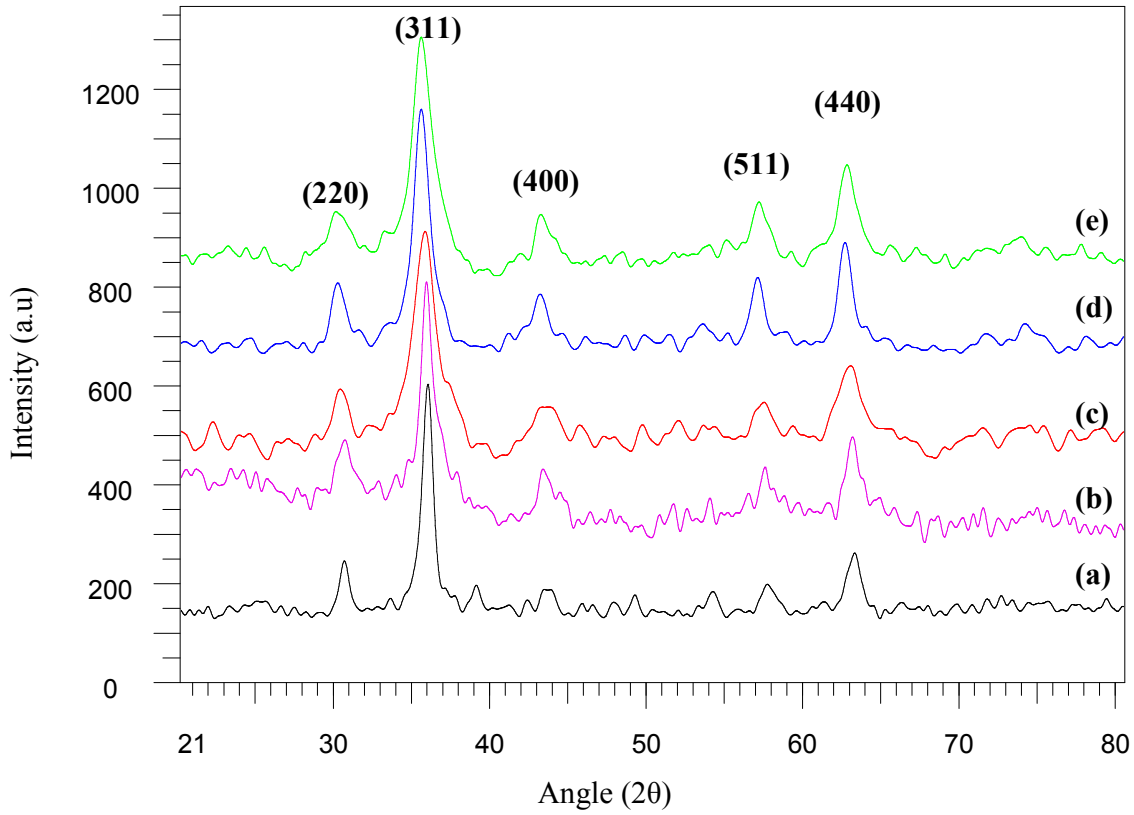

Fig 1. XRD pattern of cobalt doped cobalt ferrite ($Co_xCu_{1-x}Fe_2O_4$) where (a) x=0.0, (b) x=0.2, (c) x=0.6, (d) x= 0.8 and (e) x=1.0

RSC Advances Accepted Manuscript

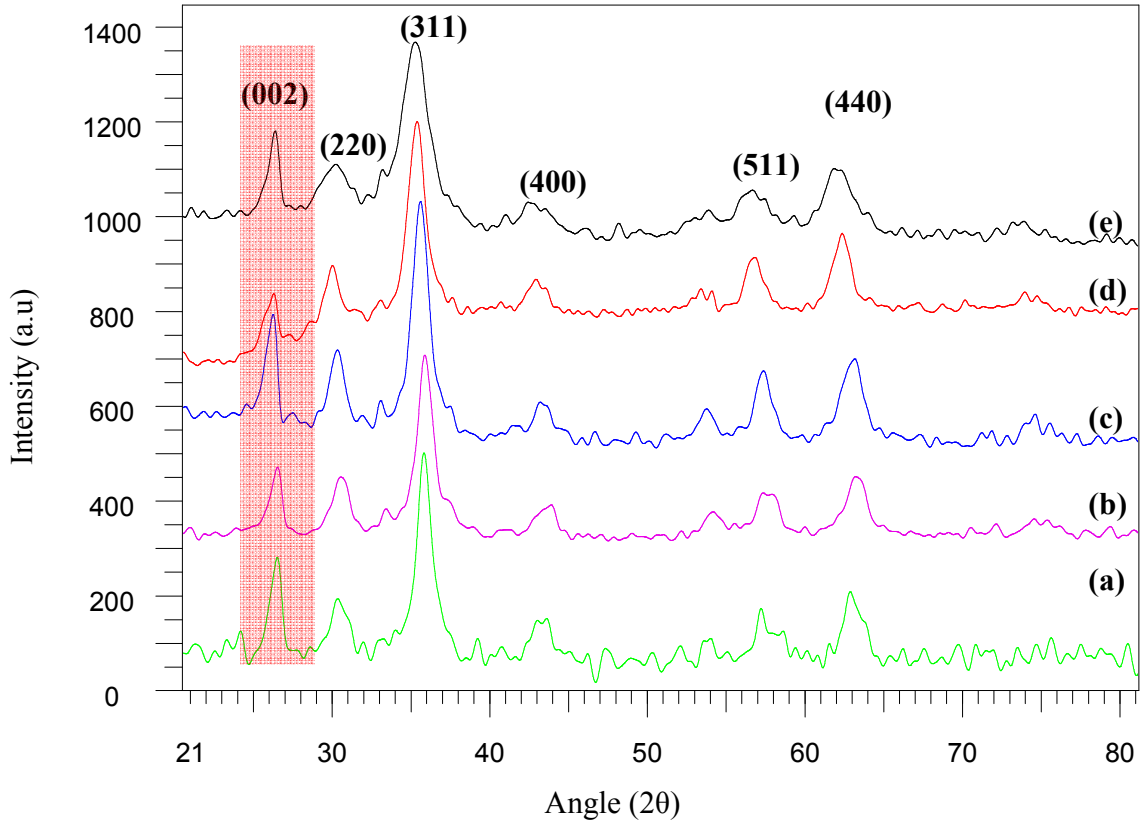

Fig 2. Powder XRD pattern of $Co_xCu_{1-x}Fe_2O_4$-MWCNTs where (a) x=0.0, (b) x=0.2, (c) x=0.6, (d) x= 0.8 and (e) x=1.0

RSC Advances Accepted Manuscript

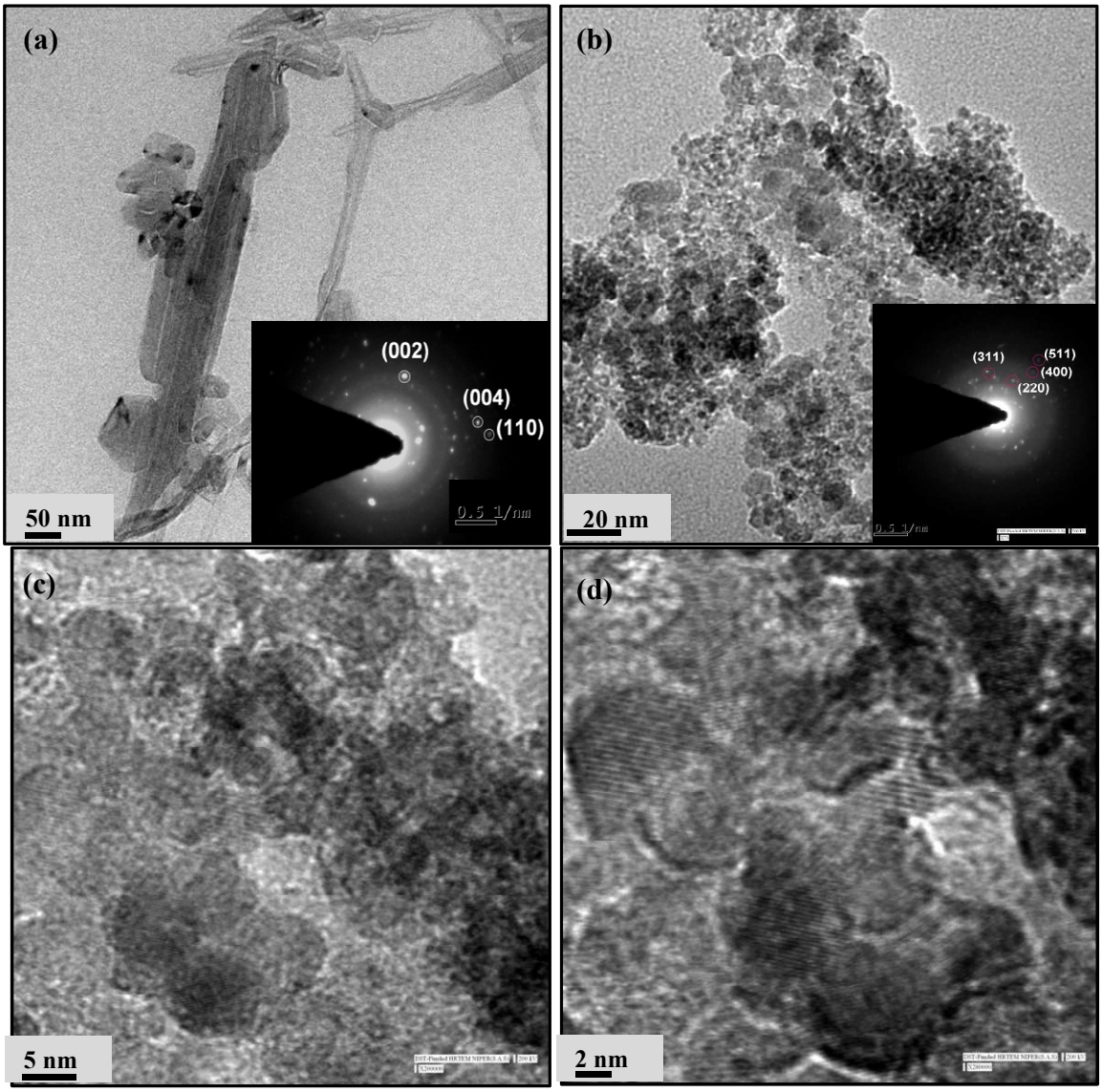

Fig 3. HR-TEM images (a) Purified and functionalized MWCNTs and inset showing the SAED pattern with (002) lattice plane (b, c and d) showing the size and shape of cobalt doped copper ferrite at different resolution.

RSC Advances Accepted Manuscript

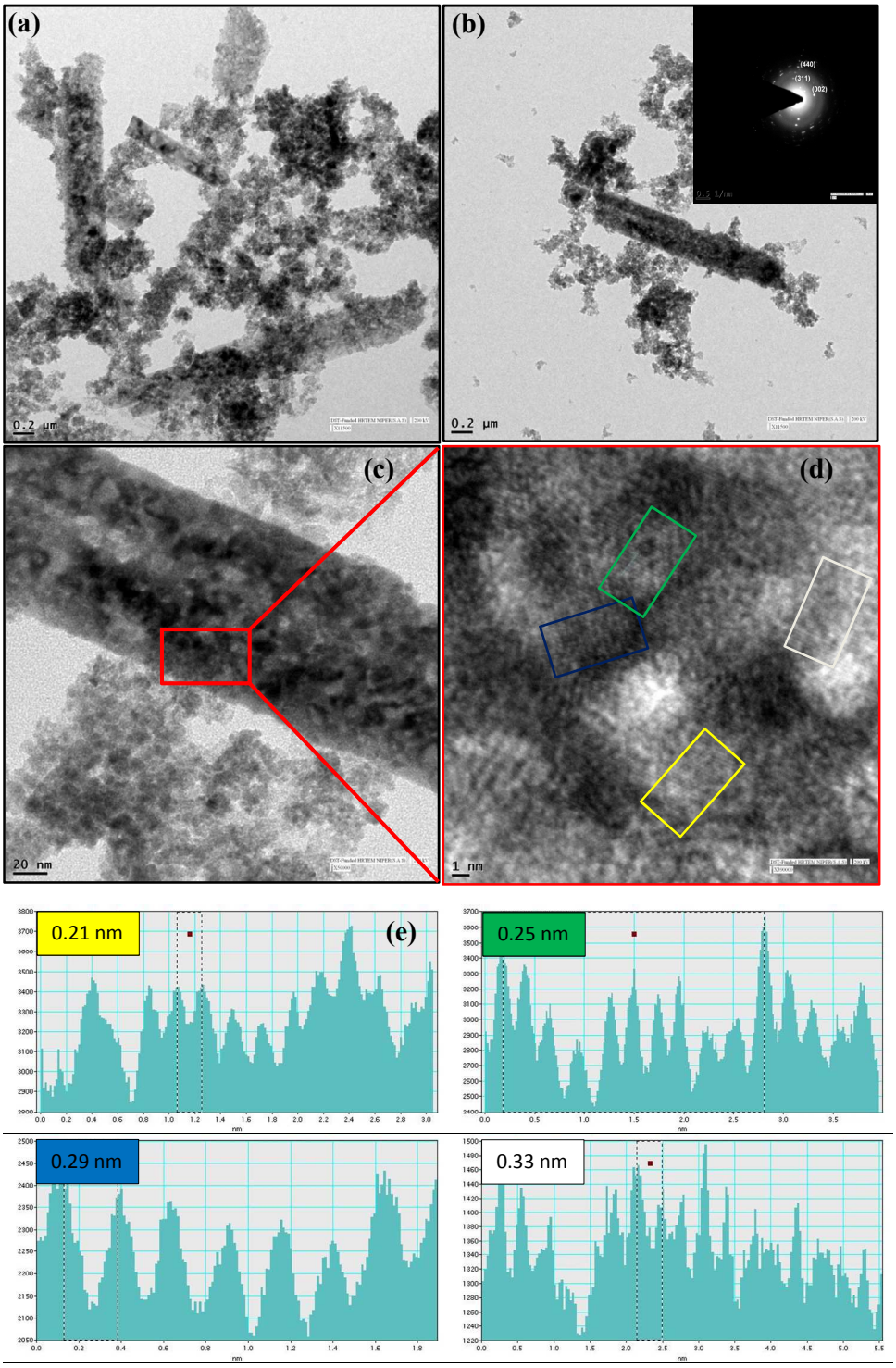

Fig. 4. HRTEM images (a, b) $Co_xC_{u1-x}Fe_2O_4$/MWCNTs nanocomposites at low resolution with inset showing the SAED pattern (c) ferrite/CNTs nanocomposites at high resolution (d) $Co_xC_{u1-x}Fe_2O_4$/MWCNTs nanocomposites showing fringe width (e) profile of frame showing the different interplaner distance of ferrite/CNTs

RSC Advances Accepted Manuscript

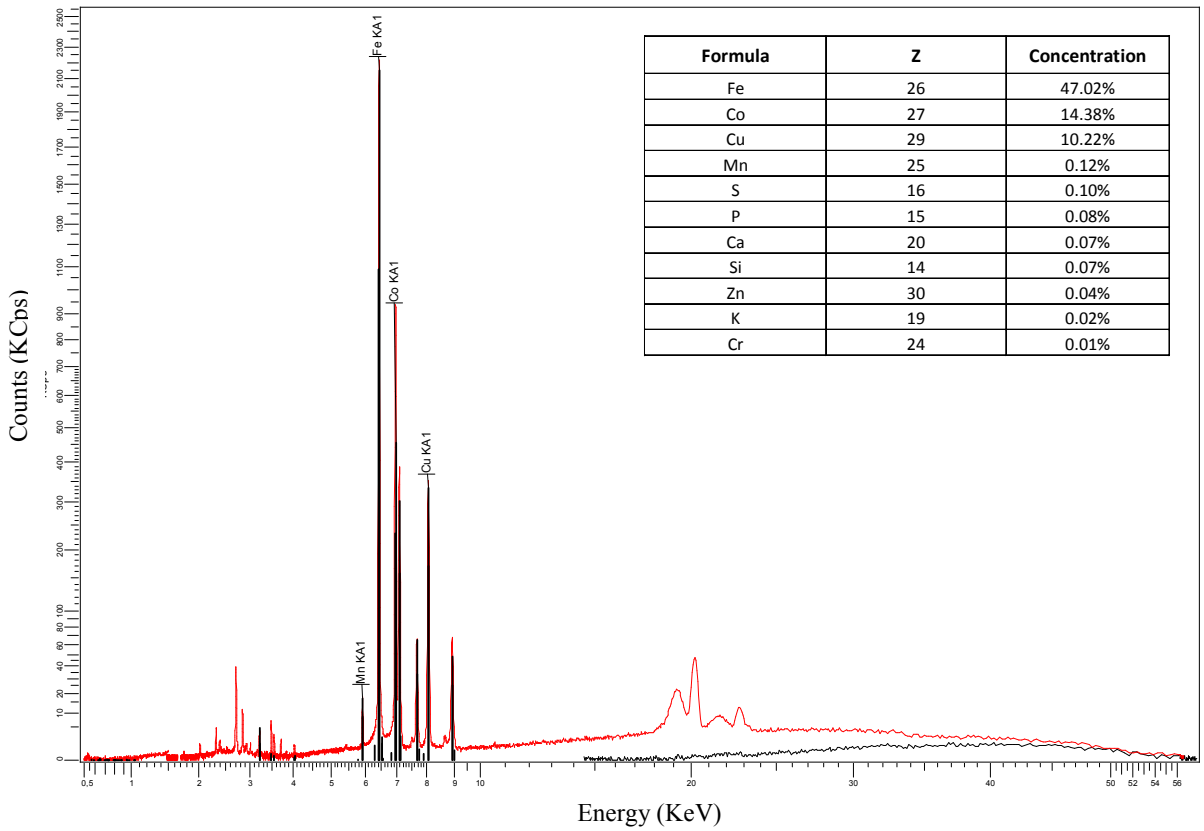

Formula	Z	Concentration
Fe	26	47.02%
Co	27	14.38%
Cu	29	10.22%
Mn	25	0.12%
S	16	0.10%
P	15	0.08%
Ca	20	0.07%
Si	14	0.07%
Zn	30	0.04%
K	19	0.02%
Cr	24	0.01%

Fig 5. Typical WDXRF spectra for the $Cu_{0.4}Co_{0.6}Fe_2O_4$-MWCNTs nanocomposite showing the elemental composition

RSC Advances Accepted Manuscript

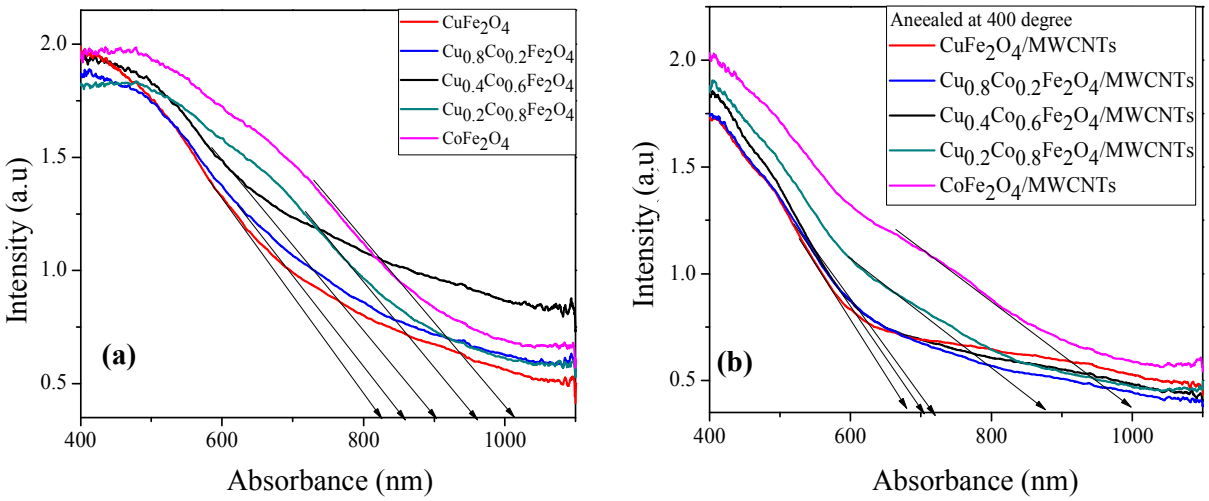

Fig 6. Diffused UV-Visible spectra of (a) cobalt doped copper ferrite nanoparticles and (b) cobalt doped copper ferrite-MWCNTs nanocomposites

RSC Advances Accepted Manuscript

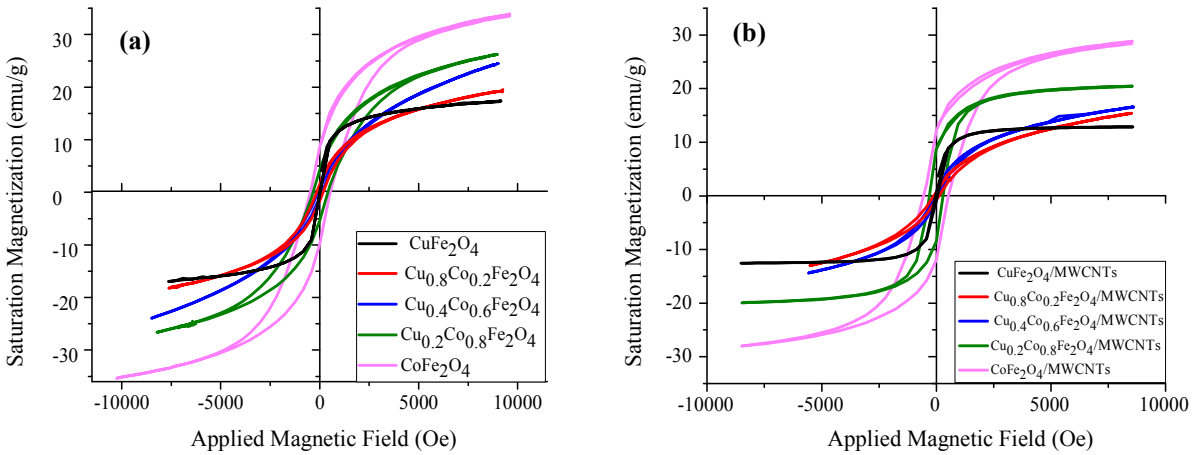

Fig 7. Magnetic hysteresis loops of (a) $Co_xCu_{1-x}Fe_2O_4$ nanoparticles and (b) $Co_xCu_{1-x}Fe_2O_4$/MWCNTs nanocomposites

RSC Advances Accepted Manuscript

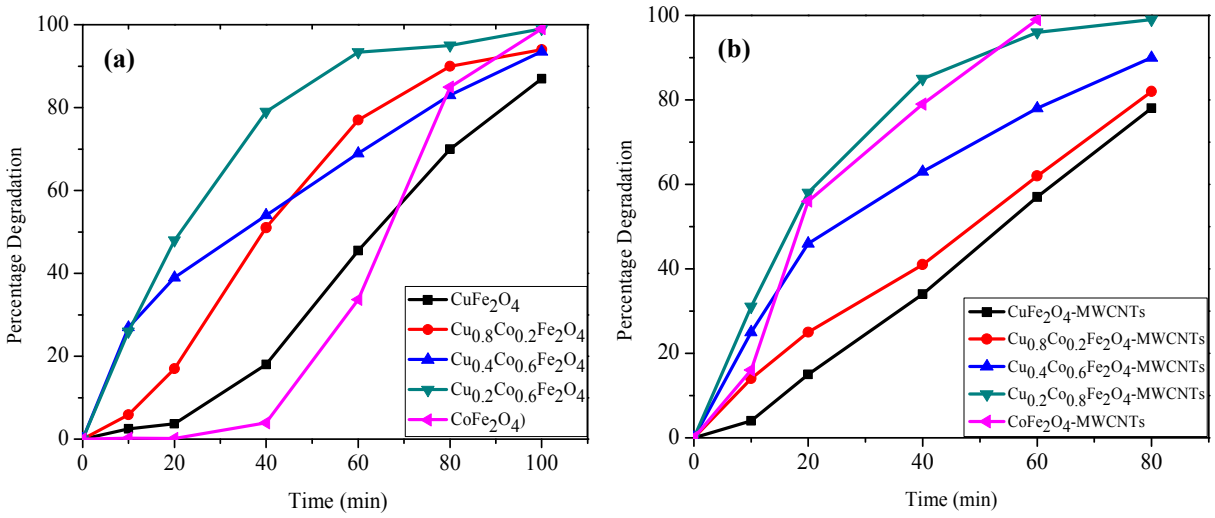

Fig 8. Degradation percentage of 50 µM Rhodamine B dye (pH= 2.5) over the time using 50 mg of (a) Cobalt doped copper ferrite nanoparticles (b) Cobalt doped copper ferrite-MWCNTs nanocomposites using 100 µL of H_2O_2.

RSC Advances Accepted Manuscript

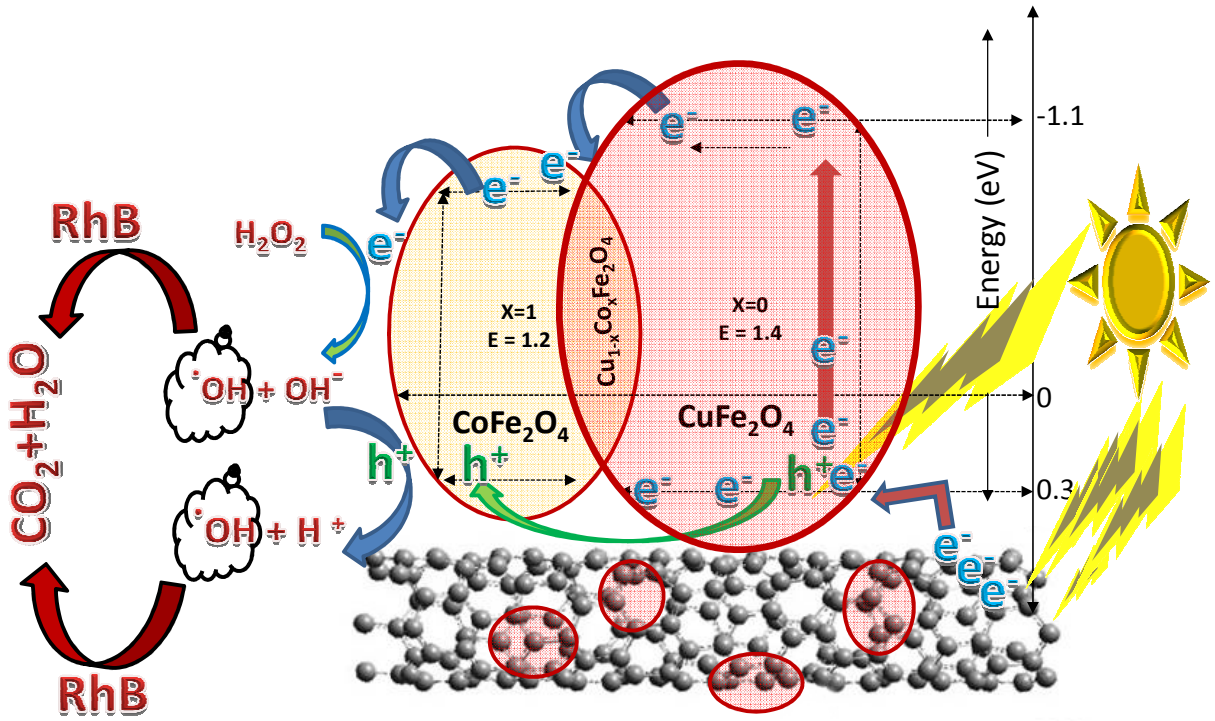

Fig 9. Energy level diagram showing the mechanistic aspect for the degradation of RhB dye

RSC Advances Accepted Manuscript